CHALMERS

Continuum Models of Active Musculature for Impact Biomechanics Simulation

HAMID KHODAEI
SALAR MOSTOFIZADEH

Continuum Models of Active Musculature for Impact Biomechanics Simulation

Research Report in Mechanical Engineering

HAMID KHODAEI
SALAR MOSTOFIZADEH

Department of Applied Mechanics
Division of Material and Computational Mechanics and Division of Vehicle Safety
CHALMERS UNIVERSITY OF TECHNOLOGY

Göteborg, Sweden 2010

Continuum Models of Active Musculature for Impact Biomechanics Simulation
HAMID KHODAEI
SALAR MOSTOFIZADEH

Cover:
Continuum Models of Active Musculature for Impact Biomechanics Simulation

Continuum Models of Active Musculature for Impact Biomechanics Simulation
Research Report in Mechanical Engineering

HAMID KHODAEI
SALAR MOSTOFIZADEH
Department of Applied Mechanics
Division of Material and Computational Mechanics and Division of Vehicle Safety
Chalmers University of Technology

Abstract

In order to obtain reliable and realistic results for a human body model in a car crash simulation, having a suitable constitutive model for muscle tissue with both passive and active properties, is of great importance.

Skeletal muscles have experimentally shown to have mechanical features including

- Anisotropy of the muscle

- Contraction of the muscle fibers due to external stimuli, known as activation, which is also length and velocity dependent.

- Non-linear and rate dependent behavior also without activation

A literature study was conducted, and many previous studies describing the active and passive muscle behavior in context of continuum mechanics were investigated. Some suitable modeling approaches were selected; then, an explicit FE formulation based on large deformation was developed, and implemented in a Matlab environment. The simulation results of the different approaches were assessed, and the most promising material model was chosen. This model is supposed to be implemented as a user material routine in LS-DYNA software using Fortran code.

The implemented model used a Hill-type relation for the active muscle behavior. For the numerical solutions in the FE analysis, the central difference scheme as an explicit method was mainly focused on.

One of the main problems in the FE analysis was instabilities occurring during the time iterations which is mainly due to the nearly incompressible material property of the muscle. In some cases, by assigning appropriate parameters and adjusting constants this problem was solved. Methods for treating such problems was tested; for instance, the reduced selective method was implemented in this thesis project, but satisfying results were not achieved.

Contents

Preface

This report presents the results from a Master's thesis project proposed by Chalmers University of Technology, at the department of Applied Mechanics, divisions of Material and Computational Mechanics and Vehicle Safety as a cross-divisional thesis in conjunction with SAFER in Lindholmen science park. The work was carried out from January to June 2010 by Hamid Khodaei and Salar Mostofizadeh as Master's students of Mechanical Engineering at Linköping University. The project was conducted under supervision of assistant professors Håkan Johansson and Karin Brolin, and Ph.D. student Jonas Östh from Chalmers University of Technology and professor Anders Klarbring from Linköping University.

Acknowledgements

1 Introduction

1.1 Background

Car crashes claim thousands of lives every year, and auto makers are devoting a remarkable budget to improve their vehicle safety. Since a crash test with a real vehicle is complicated and expensive, manufacturers try to use crash simulations, instead of some real tests, to investigate their products' safety issues. Increasing vehicle safety requirements and tough regulations in recent years have made it necessary to conduct more detailed and realistic crash simulations in pre-crash phase as well as crash phase. To study the possible injuries of the vehicle occupants during a crash simulation, using a human body model (HBM) with biofidelic behavior, which also includes the muscles, is of importance. As the pre-crash phase is significantly longer than the crash phase, there is a need to represent the active behavior of the vehicle occupants in this phase. A short time before a car crash, drivers usually react to what they see, so that when the crash happens, some muscles are in activated state (in addition to all muscles that are in various degrees of activation in order to maintain the driver's body position). This means that a totally different mechanical behavior of the muscle should be expected in such cases. To describe the active and passive behavior of the muscles and include them in the crash simulations, a constitutive model is required to represent these mechanical behaviors, and meanwhile it should be capable of being implemented in finite element (FE) formulations, as well as commercial FE softwares such as LS-DYNA [1].

The aim of this Master's thesis was to find a constitutive model for the skeletal muscle, representing both active and passive properties, in a continuum mechanics framework. To find such constitutive models, a comprehensive literature study was required to be done in order to investigate different approaches to material modeling, FE formulations and numerical schemes. After comparing different material models and their behavior in the Matlab environment, the most satisfying material model should be used to develop a new user-defined material routine in LS-DYNA, where crash simulations with the HBM is supposed to be executed.

Since the model is aimed at pre-crash and possibly also in-crash events, rapid deformations can be expected. This makes it necessary to take into account the rate dependency of the muscle material. Furthermore, a dynamic formulation should be used due to presence of inertia forces. In many previous studies of muscle modeling (cf. Section 4.5), the viscous part of the constitutive model was ignored and FE simulations mainly were performed under quasi-static condition.

1.2 Method

Having found some suitable material models through literature study, a Matlab code was developed to study the behavior of the constitutive equations, in which a simple symmetrically fusiform muscle model composed of 8-node solid elements was used for testing. The FE formulation used in the Matlab environment was based on the explicit method, which is suitable for the simulation of fast events. This is the method that is also used by LS-DYNA which is a commercial FE software frequently used for car crash simulations. The purpose of simulations with Matlab codes was to provide an environment, where different material

models and different problem setups were possible to be implemented, as in LS-DYNA it is not always easy to change all aspects of the simulation.

Many simulations run in Matlab led to unstable results. This was one of the obstacles in the project, because there was an uncertainty about the cause of instability. Indeed, there are many factors that results depend on; for example, choosing the parameters and constants could be crucial as there is usually no reliable source for them, which was due to the lack of experimental data for the skeletal muscles. Therefore, sometimes parameters were chosen based on estimations.

1.3 Muscle physiology

According to Fung [2], the units of skeletal muscle are the muscle fibers, each of which is a single cell provided with many nuclei. These fibers are arranged in bundles of various sizes within the muscle. Connective tissue fills the spaces between the muscle fibers within a bundle. Each bundle is surrounded by a stronger connective tissue sheath; and the whole muscle is again surrounded by an even stronger sheath.

A skeletal muscle fiber is elongated, having a diameter of $10 - 60$ μm, and a length usually of several millimeters to several centimeters; but sometimes the length can reach 30 cm in long muscles. The fibers may stretch from one end of muscle to another, but often extend only part of the length of the muscle, ending in tendinous or other connective tissue intersections. Figure 1.1 illustrates the muscle structure.
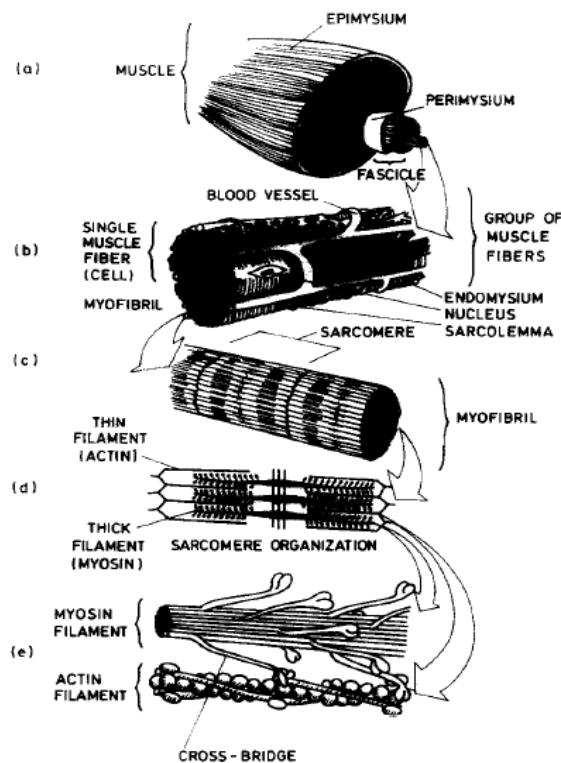
Figure 1.1: Structure of skeletal muscle (taken from Fung [2]).

The flattened nuclei of muscle fibers lie immediately beneath the cell membrane. The cytoplasm (the cell substance between the cell membrane and the nucleus) is divided into myofibrils. Each myofibril is composed of arrays of myofilaments. These are divided transversely into serially repeating sarcomeres, with the exact length dependent on the force acting in the muscle and the state of excitation. Two types of myofilaments are distinguishable in each sarcomere, fine ones, that are actin molecules, and the thick ones, that are myosin molecules.
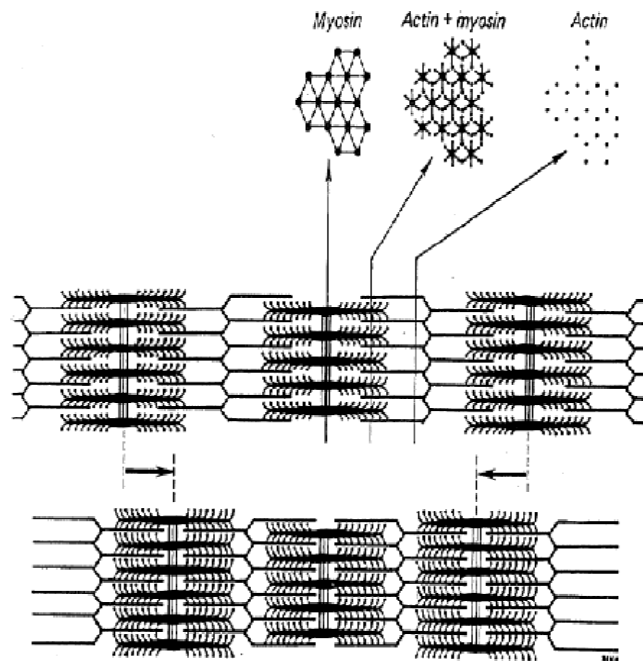
Figure 1.2: Micro structure of the contractile muscle tissue (taken from Fung [2]).

As can be seen in Figure 1.2 each myosin filament consists of number of molecules and each molecule consists of a long tail piece and a head. These filaments are called cross-brigdes and are responsible for the active force generation of the muscle tissue in a process where the head of the myosin molecule bends when the muscle is activated [2].

1.3.1 Contraction of skeletal muscle bundles

A muscle has many fibers, which are stimulated by motor neurons. Each motor neuron may innervate many muscle fibers, but all the muscle fibers are not stimulated at the same time. The total force of contraction of a muscle depends on how many muscle fibers are stimulated, and partial activation is achieved when only part of the fibers are activated.

2 Constitutive modeling of muscles

One of the objectives of this thesis is to define a material model in a continuum framework in such a way that active and passive properties of muscle tissue can be represented. In the literature, there are different models of muscle tissue that can be used as a base for a continuum model. Hill's model is one of the most popular muscle models in this regard. This model is a whole muscle model with one degree of freedom with force-length and force-velocity relations. Furthermore, as we are dealing with large deformations, specific set of formulations is required. Also, fast deformations of the muscle implies that the rate dependent behavior of the muscle material should be considered.

2.1 Hill's three-element model

Hill's model represents the complete muscle behavior with three structural elements. Two elements are arranged in series: a contractile element, which at rest is freely extensible, but when activated is capable of shortening, and an elastic element arranged in series with the contractile element (CE) [2]. To account for the elasticity of the muscle at rest (i.e. its passive properties), a parallel elastic element is added. The contractile element is identified with the sliding actin-myosin molecules, and the generation of active tension with the number of active cross-bridges between them.
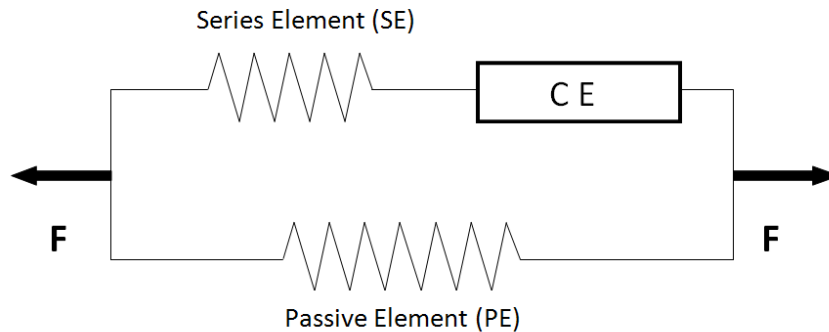
Figure 2.1: Hill's three element model.

2.1.1 Force-length relation

From experiments [3] the active force generated by the muscle has a dependency on the length of the muscle, and has its maximum value at the optimal muscle length L_{opt}, which can be assumed to be the resting length of the muscle [4], but in reality L_{opt} often varies a little bit from the resting length. The force-length relation can be expressed as [3]

$$f_L(L) = e^{-\left(\frac{\left(\frac{L}{L_{opt}}-1\right)}{c_{sh}}\right)^2} \tag{2.1}$$

where L is the total muscle length and C_{sh} is a shape factor.
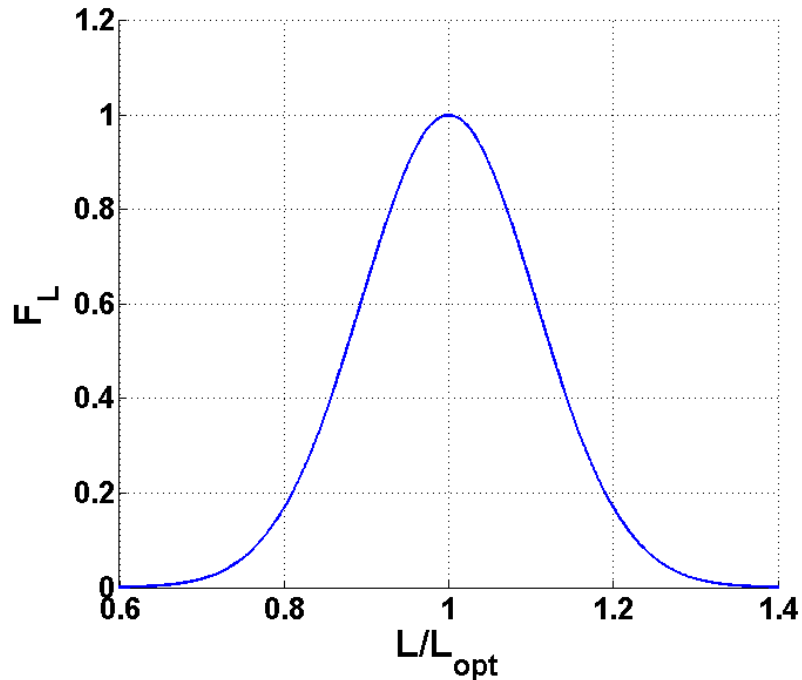
Figure 2.2: Force-length relation.

2.1.2 Force-velocity relation

It has also been observed in experiments that the active force generated by the muscle depends on the shortening and lengthening velocity. With increasing shortening velocity the generated force will be reduced. Also, with increase of lengthening velocity the muscle force will respond in an asymptotic manner as shown in Figure 2.3. This relation is presented as the following equation [3]

$$
f_v(V) = \begin{cases} 0 & \nu \leq -1 \\[2mm] \frac{1+\nu}{1-\frac{\nu}{C_{short}}} & -1 < \nu \leq 0 \\[2mm] \frac{1+\nu\frac{C_{mvl}}{C_{leng}}}{1+\frac{\nu}{C_{leng}}} & \nu > 0 \end{cases} \qquad , \qquad \nu = \frac{V}{V_0} \tag{2.2}
$$

where ν is the normalized shortening velocity with respect to the maximum shortening velocity of the muscle V_0. For shortening velocities larger than V_0 the muscle is unable to produce any force.
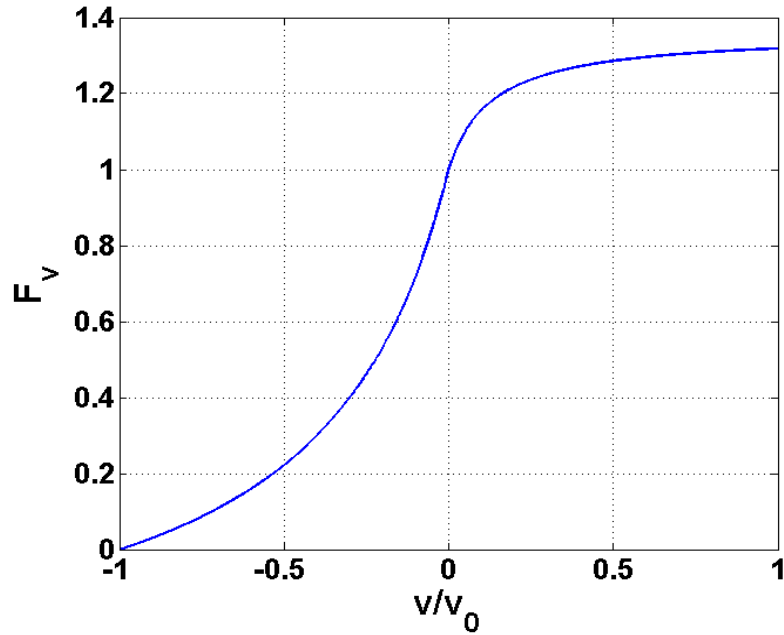
Figure 2.3: Force-velocity relation.

2.1.3 Total muscle force

The total active force generated in a Hill-based contractile element (CE) can be expressed as

$$F_{CE}(L,V) = a(t)\sigma_0 F_L(L) F_V(V) \tag{2.3}$$

where $a(t)$ is a function of time, representing the state of activation, which takes a value between 0 and 1, and σ_0 is the maximum isometric stress of the muscle [5].

Since the force in the contractile element F_{CE} will be the same as the force in the series element, F_{SE} can be ignored; consequently, the total muscle force in a muscle can be expressed as the sum of the forces in the contractile element and the passive element (PE)

$$F = F_{PE} + F_{CE} \tag{2.4}$$
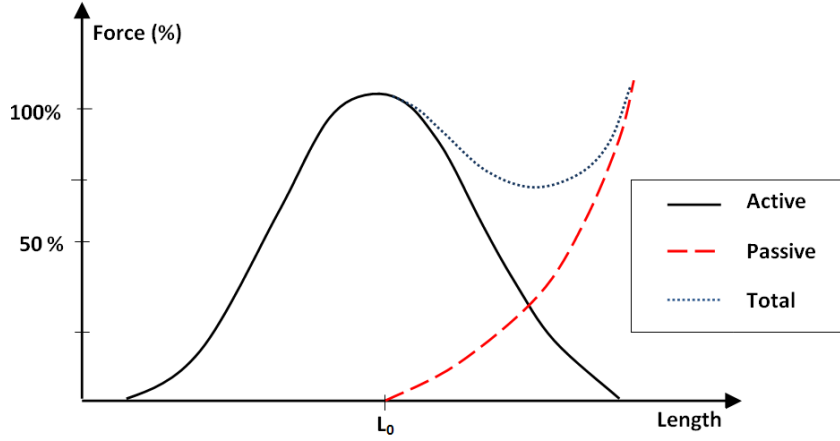
Figure 2.4: Schematic force-length relation of the muscle for active, passive and total muscle force.

2.2 Activation dynamics models

The muscle activation level is mainly governed by the Ca^{2+} ion concentration in the muscle tissue. Increased intracellular calcium Ca^{2+} concentration (600–800 nM) causes contraction and decreased Ca^{2+} concentration (100 nM) leads to relaxation of the muscle. The release of Ca^{2+} in the cells can be initiated by neural impulses [6]. A mechanochemical approach was used by Stålhand et al. [7] to introduce a thermodynamically consistent constitutive relations based on the chemical state variable driven by Ca^{2+} concentration.

Guccione et al. [8] also proposed relations for muscle activation dynamics based on calcium ion concentration and sarcomere length. This model is intended for heart muscle which its activation and deactivation occurs periodically. Their suggested relation for the active stress is

$$\sigma = \sigma_0 \frac{Ca_0^2}{Ca_0^2 + ECa_{50}^2} a(t) \tag{2.5}$$

where Ca_0^2 and ECa_{50}^2 are parameters related to the Ca^{2+} state in the muscle. The fraction $Ca_0^2/(Ca_0^2 + ECa_{50}^2)$ captures the stress contribution of $F_V F_L$ in the Equation 2.3.

As for activation and deactivation functions, $a(t)$ in Equation 2.3, they suggested the following relation which is related to cyclic excitation of the heart muscle.

$$a(t) = \frac{1}{2}(1 - cos\omega) \tag{2.6}$$

where ω adjusts the activation-deactivation curve based on the peak stress and zero stress times. In case of skeletal muscles, this curve depends on the neural excitation.

Another formulation for activation and deactivation of skeletal muscle was introduced by Martins et al. [9] accounting to the delay between neural excitation and activation of the muscle. Figure 2.5 shows activation and deactivation curves

$$\dot{a}(t) = \frac{1}{\tau_{rise}}(1 - a(t))u(t) + \frac{1}{\tau_{fall}}(a_{min} - a(t))(1 - u(t)) \tag{2.7}$$
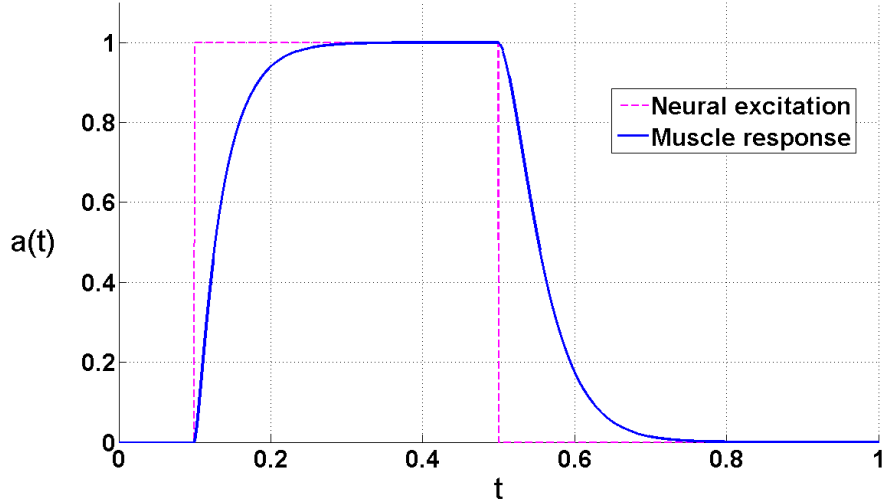
Figure 2.5: Activation and deactivation curve of muscle exposed to a neural excitation in form of a step function.

In the above equation τ_{rise} and τ_{fall} are activation and deactivation time constants, $u(t)$ is a function representing the neural excitation ranging from 0 to 1, a_{min} is the minimum level of activation and $a(t)$ is the activation ranging from $a_{min} \geq 0$ to 1.

2.2.1 Huxley model, hypotheses of the cross-bridge theory

The Huxley model describes the contraction of the muscles based on the cross-bridges and the interaction of actin and myosin filaments. It is assumed that during muscle contraction a fraction of all cross-bridges is attached, and every attached cross-bridge has its own dimensionless attachment length ξ. The distribution of attached cross-bridges with respect to their length is given by a function $n(\xi, t)$ [10] [11].

The active muscle stress depends on the distribution of the attached cross-bridges, and the cross-bridge force depends linearly on the length of the cross-bridge. The active Cauchy stress σ_a generated by all cross-bridges in a sarcomere is expressed as

$$\sigma_a(t) = \sigma_0 \lambda \int_{-\infty}^{\infty} \xi n(\xi, t) d\xi = c_a \lambda Q_1(t) \tag{2.8}$$

where Q_1 is the first moment of the function $n(\xi, t)$, σ_0 is the maximum isometric stress, and λ is the stretch in the fiber direction.

In a number of studies, a two-state Huxley model has been used. According to this model, cross-bridges are either attached or detached. According to Oomens et al. [10] [11], this type of model is suitable for slow events, but not for the rapid events which is the case with the present study.

2.3 Muscle test cases

To investigate the mechanical properties of the muscles, there are some standard test cases in which the active properties of muscle tissue is assessed. For the results of the numerical

model to be validated according to experimental data, it is necessary to impose similar conditions as in these test cases in the FE simulations. The most common test cases are isometric, isokinetic and isotonic tests.

2.3.1 Isometric test

In this test the muscle is fixed in both ends. The muscle can be fixed at a reference length, resting length, or can be fixed in a lengthened or shortened state in which a passive stress proportional to the stretch will be developed in the muscle. By activation of the muscle, the total amount of force can be recorded. By performing this test for different values of stretch, one can obtain a force-length curve of the muscle, similar in shape to that in Figure 2.2 (cf. Section 2.1.1).

2.3.2 Isokinetic test

To study the force-velocity relation of the muscle, a constant velocity can be applied to one end of the muscle, and meanwhile the amount of the force in the activated muscle can be registered. Different shortening and lengthening velocities with activation leads to different force levels. Using these forces a force-velocity curve can be achieved (cf. Section 2.1.2).

2.3.3 Isotonic test

Applying a constant force to the muscle, eccentric, lengthening muscle while activated, and concentric, shortening muscle while activated, movements of the muscle can be studied. This type of test was not focused on much in this project.

2.4 Continuum mechanics and large deformations

Since the muscle is a relatively soft material that will undergo significant deformations, a framework capable of handling large deformations is needed. In the context of non-linear continuum mechanics some basic formulations have been provided. The formulations and notations are taken from Belytschko et al. [12].

2.4.1 Preliminaries, strain and stress measures

Deformation gradient $\boldsymbol{F}$ For an arbitrary displacement of a body with reference coordinate, $\boldsymbol{X}$, and current configuration $\boldsymbol{x}$ with a mapping function ϕ between reference and current configuration we have:

$$\boldsymbol{x} = \phi(\boldsymbol{X}), \qquad \boldsymbol{F} = \frac{\partial \phi}{\partial \boldsymbol{X}} = \frac{\partial \boldsymbol{x}}{\partial \boldsymbol{X}} \tag{2.9}$$

And the Jacobian is defined as follows:

$$J = det(\boldsymbol{F}) \tag{2.10}$$
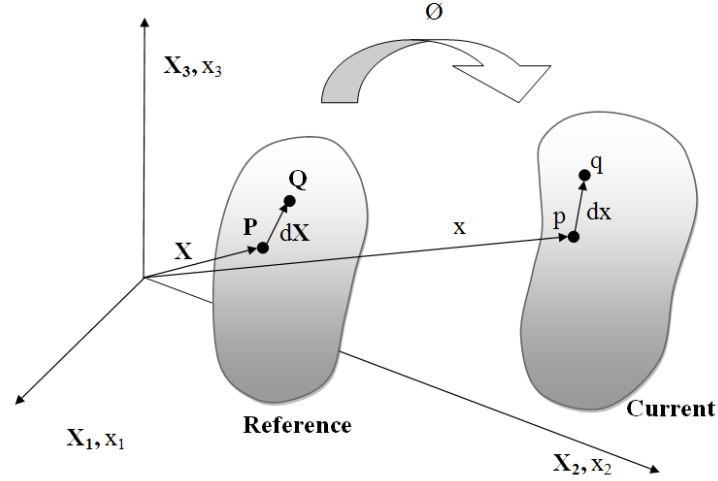
Figure 2.6: A general motion of points P and Q from reference to current configuration.

Green's deformation tensor $\boldsymbol{C}$

$$\boldsymbol{C} = \boldsymbol{F}^T \cdot \boldsymbol{F} \tag{2.11}$$

Lagrangian finite strain (Green strain) tensor $\boldsymbol{E}$

$$\boldsymbol{E} = \frac{1}{2}(\boldsymbol{F}^T \cdot \boldsymbol{F} - \boldsymbol{I}) \quad or \quad \boldsymbol{E} = \frac{1}{2}(\boldsymbol{C} - \boldsymbol{I}) \tag{2.12}$$

Rate-of-Deformation $\boldsymbol{D}$ This is a rate measure of deformation which is also called velocity strain. We first define the velocity gradient $\boldsymbol{L}$ by

$$\boldsymbol{L} = \frac{\partial \boldsymbol{v}}{\partial \boldsymbol{x}} = (\nabla \boldsymbol{v})^T \tag{2.13}$$

The rate-of-deformation $\boldsymbol{D}$ is defined as the symmetric part of $\boldsymbol{L}$:

$$\boldsymbol{D} = \frac{1}{2}(\boldsymbol{L} + \boldsymbol{L}^T) \tag{2.14}$$

Rate-of-Deformation in terms of $\dot{\boldsymbol{E}}$

$$\boldsymbol{L} = \frac{\partial \boldsymbol{v}}{\partial \boldsymbol{x}} = \frac{\partial \boldsymbol{v}}{\partial \boldsymbol{X}} \cdot \frac{\partial \boldsymbol{X}}{\partial \boldsymbol{x}} \tag{2.15}$$

From the above equation the following expressions can be derived

$$\dot{\boldsymbol{F}} = \frac{\partial \boldsymbol{v}}{\partial \boldsymbol{X}}, \quad \boldsymbol{F}^{-1} = \frac{\partial \boldsymbol{X}}{\partial \boldsymbol{x}} \to \boldsymbol{L} = \dot{\boldsymbol{F}} \cdot \boldsymbol{F}^{-1} \tag{2.16}$$

Finally we have

$$\boldsymbol{D} = \boldsymbol{F}^{-T} \cdot \dot{\boldsymbol{E}} \cdot \boldsymbol{F}^{-1} \tag{2.17}$$

Stress measures In order to formulate the non-linear problem, two kinds of stress measures have been considered :

- The Cauchy stress, $\boldsymbol{\sigma}$, which is defined in the current configuration
- The second Piola-Kirchhoff (PK2) stress tensor, $\boldsymbol{S}$, which is defined in the reference configuration

The transformation of the stresses between current and reference configuration can be defined as follows

Push-forward operation:
$$\boldsymbol{\sigma} = J^{-1} \boldsymbol{F} \cdot \boldsymbol{S} \cdot \boldsymbol{F}^T \tag{2.18}$$

Pull-backward operation:
$$\boldsymbol{S} = J \boldsymbol{F}^{-1} \cdot \boldsymbol{\sigma} \cdot \boldsymbol{F}^{-T} \tag{2.19}$$

2.4.2 Hyper-elasticity

The non-linear elastic behavior of the muscle can be expressed as a constitutive equation in the context of hyper-elasticity, in which the stresses can be derived from the stored energy function. The material is called hyper-elastic if the work done by the stresses is path independent, i.e. it depends only on the initial and final configuration. The elastic potential energy Ψ can be defined as [13]

$$\Psi(\boldsymbol{F}(\boldsymbol{X}), \boldsymbol{X}) = \int_{t_0}^{t} P(\boldsymbol{F}(\boldsymbol{X}), \boldsymbol{X}) \mathbf{:} \dot{\boldsymbol{F}} \, dt \tag{2.20}$$

Consequently the Lagrangian constitutive equation is

$$\boldsymbol{S}(\boldsymbol{C}(\boldsymbol{X}), \boldsymbol{X}) = 2\frac{\partial \Psi}{\partial \boldsymbol{C}} = \frac{\partial \Psi}{\partial \boldsymbol{E}} \tag{2.21}$$

In case of incompressibility where we have the constraint $J = 1$, the constitutive equation becomes

$$\boldsymbol{S} = 2\frac{\partial \Psi(\boldsymbol{C})}{\partial \boldsymbol{C}} + \gamma J \boldsymbol{C}^{-1} \tag{2.22}$$

Where parameter γ is a scalar that represents hydrostatic pressure in case of pure incompressibility. Introducing the distortional part of energy function $\hat{\Psi}$, the above equation becomes

$$\boldsymbol{S} = 2\frac{\partial \hat{\Psi}(\boldsymbol{C})}{\partial \boldsymbol{C}} + p J \boldsymbol{C}^{-1} \tag{2.23}$$

- **Neo-hookean material**

  This is a special simple case of the hyperelastic materials with two material parameters of λ μ that can be easily determined. In the compressible case the energy function is as follows

$$\Psi = \frac{\mu}{2}(I_{\mathbf{C}} - 3) - \mu ln J + \frac{\lambda}{2}(ln J)^2 \qquad (2.24)$$

Where I_C is the first invariant of tensor C, and in the case of incompressibility the above relation simplifies to

$$\Psi(\boldsymbol{C}) = \frac{1}{2}\mu(tr\boldsymbol{C} - 3) \qquad (2.25)$$

2.5 Viscoelasticity

The muscle model we are working on, is supposed to be implemented in car crash simulations which means that very fast deformations should be taken into account. This means that, unlike many previous works, viscous forces will not be possible to ignore. As a result having a constitutive model based on viscoelastic properties seems to be necessary.

- **Maxwell model** This simple model is one of the most common rheological models which is composed of a spring and a viscous dashpot arranged in series as depicted in Figure 2.7.

Figure 2.7: Maxwell model.

In most cases a generalized form of the Maxwell model is used, in which a group of single Maxwell elements are gathered in parallel (Figure 2.8). Usually by assigning desired values to the elasticity or viscosity coefficients different material behaviors of the model can be achieved. For example, by setting the μ value to infinity in one of the elements in Figure 2.8 the corresponding element will be changed to a purely elastic element.

2.5.1 Viscoelastic constitutive model for the implicit method

Based on the internal variables, an alternative choice of viscoelastic constitutive formulation for a transversely isotropic material presented by Kaliske [14] have been introduced here. This model is developed based on viscoelastic hereditary relation and second Piola-Kirchhofff stress tensor, and can be implemented in an implicit time integration. This can be a good basis for the further development of the project for a new implicit formulation.

$$\boldsymbol{S}(\boldsymbol{C}, \boldsymbol{K}) = \boldsymbol{S}_0 + \sum_{j=1}^{n} \boldsymbol{H}_j \qquad (2.26)$$

A linear rate equation for a generalized Maxwell model, defines the constitutive relation between the internal viscoelastic stress variables H_j and the elastic stress rate $\dot{S}_0$ which can be expressed as
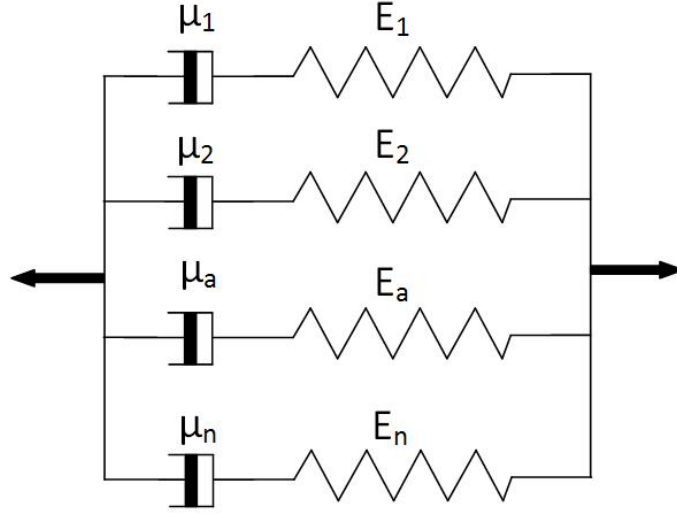
Figure 2.8: Generalized Maxwell model.

$$\dot{\boldsymbol{H}}_j + \frac{1}{\tau_j}\boldsymbol{H}_j = \boldsymbol{\Gamma}_j\dot{\boldsymbol{S}}_0 \tag{2.27}$$

The hereditary integral introducing the time dependency is

$$\boldsymbol{H}_j(\boldsymbol{C},\boldsymbol{K}) = \int_0^t \boldsymbol{\Gamma}_j(\boldsymbol{K})\exp\left(-\frac{t-t^*}{\tau_j}\right)\frac{\partial \boldsymbol{S}_0(\boldsymbol{C},\boldsymbol{K})}{\partial t^*}dt^* \tag{2.28}$$

Discretizing over time step Δt we will have

$$\boldsymbol{H}_j^{n+1} \approx \exp\left(-\frac{\Delta t}{\tau_j}\right)\boldsymbol{H}_j^n + \boldsymbol{\Gamma}_j\frac{1-\exp(-(\Delta t/\tau_j))}{(\Delta t/\tau_j)}[\boldsymbol{S}_0^{n+1} - \boldsymbol{S}_0^n] \tag{2.29}$$

To derive the tangent moduli, derivative of the stress tensor can be computed

$$\boldsymbol{A}^{n+1} = 2\frac{\partial \boldsymbol{S}^{n+1}}{\partial \boldsymbol{C}^{n+1}} = \left\{\boldsymbol{I} + \sum_{j=1}^n \boldsymbol{\Gamma}_j(\boldsymbol{K})\frac{1-\exp(-(\Delta t/\tau_j))}{(\Delta t/\tau_j)}\right\}\boldsymbol{A}_0^{n+1}(\boldsymbol{C},\boldsymbol{K}) \tag{2.30}$$

Where τ_j, relaxation time, and Γ_j, a fourth order relaxation tensor are material parameters. Using this formula an approximate update of the anisotropic viscoelastic stress variables can be obtained. The relaxation function tensor can be determined using

$$\boldsymbol{\Gamma}(t) = \boldsymbol{I} + \sum_{j=1}^n \boldsymbol{\Gamma}_j\exp(-t/\tau_j) \tag{2.31}$$

and $\boldsymbol{A}_0^{n+1}$ is nonlinear elastic material tensor.

2.5.2 Hyper-elastic material model - transversely isotropic materials

The muscle structure can be considered as transversely isotropic material in which an isotropic material is reinforced by fibers with a mean direction, and the material property

is assumed to remain unchanged transverse to the mean fiber direction n. Freed et al. [15] developed a constitutive model for soft tissues with dispersed fiber direction, and a dispersion matrix $\boldsymbol{K}$ for approximation of mean fiber direction was presented. To derive the constitutive equation, the free energy functions were expressed based on the theory of invariants, in which five invariants of the $\boldsymbol{C}$ matrix were used to describe the material with transversely isotropy. Based on the work by Freed et al.[15], Olsson [16] presented the following formulation, which was used for the constitutive model of muscle in the MatLab codes (excluding the viscous part). Defining the isochoric-volumetric split by introducing $\bar{\boldsymbol{F}} = J^{-1/3}\boldsymbol{F}$ and $\bar{\boldsymbol{C}} = \bar{\boldsymbol{F}}^{T}\bar{\boldsymbol{F}}$, the strain energy density can be decoupled as

$$\varrho_0 \Psi(\boldsymbol{C}) = \widetilde{\psi}(J) + \overline{\psi}(\bar{\boldsymbol{C}}) + \widehat{\psi}(\boldsymbol{K}, \bar{\boldsymbol{C}}) \tag{2.32}$$

where $\widetilde{\psi}$, $\overline{\psi}$ and $\widehat{\psi}$ are the volumetric, deviatoric-isotropic and deviatoric-anisotropic strain energies, respectively. It is noteworthy that the volumetric part of the stored energy function depends only on J. Besides, this energy function should be strictly convex, and has a minimum at $J = 1$ [17].

The functional form used for the dilational strain-energy model is:

$$\widetilde{\psi}(J) = \kappa\frac{1}{2}(J-1)^2 \tag{2.33}$$

where κ is the bulk modulus. For isotropic contribution to the deviatoric strain energy we have:

$$2\overline{\psi}(\bar{\boldsymbol{C}}) = \mu\frac{1}{4}(tr\bar{\boldsymbol{C}} + tr\bar{\boldsymbol{C}}^{-1} - 6) \tag{2.34}$$

The anisotropic contribution to the deviatoric strain energy can be obtained from the following integral as the area under the force-displacement curve

$$\widehat{\psi}(\boldsymbol{K}, \bar{\boldsymbol{C}}) = \int_{1}^{[tr(\boldsymbol{K}\bar{\boldsymbol{C}})]^{1/2}} \sigma(\lambda)d\lambda \tag{2.35}$$

where σ represents the passive fiber stress, and $\bar{C}$ is the isochoric(deviatoric) part of the Cauchy-Green deformation tensor. Since it is assumed that we have just a single fiber direction in the muscle (no fiber splay), the dispersion matrix K can be simplified as $\boldsymbol{K} = n_0 \otimes n_0$ for the unit fiber direction vector n_0 in the reference configuration. Consequently, the parameter λ, here can be assumed to be the stretch in fiber direction, defined as $\lambda = \sqrt{tr[K\bar{C}]}$.

Concerning the passive fiber stress, σ, a simple exponential model has been used [16]

$$\sigma = C_1\left(e^{\frac{C_2}{2}(\lambda^2-1)} - 1\right) \tag{2.36}$$

where parameters C_1 and C_2 are determined through curve fitting with respect to experimental data curves in Figure 2.9.

The stress $\boldsymbol{S}$ can be derived from the free energy function

$$\boldsymbol{S} = 2\frac{\partial\psi}{\partial\boldsymbol{C}} \tag{2.37}$$

and the constitutive equation assigned to capture hyper-elastic and fiber contributions without taking into account viscous effect is:

$$\boldsymbol{S} = \kappa J(J-1)\boldsymbol{C}^{-1} + \mu J^{-2/3} DEV\left[\frac{1}{4}(\boldsymbol{I} - \bar{\boldsymbol{C}}^{-2})\right] + J^{-2/3}[\sigma(\lambda)+\epsilon(\lambda,\dot{\lambda})]DEV[\boldsymbol{K}] \quad (2.38)$$

where the function ϵ in this equation defines the active fiber model, and DEV is the Lagrangian deviatoric operator:

$$DEV[\bullet] = (\bullet) - \frac{1}{3}tr((\bullet)\boldsymbol{C})\boldsymbol{C}^{-1} \quad (2.39)$$
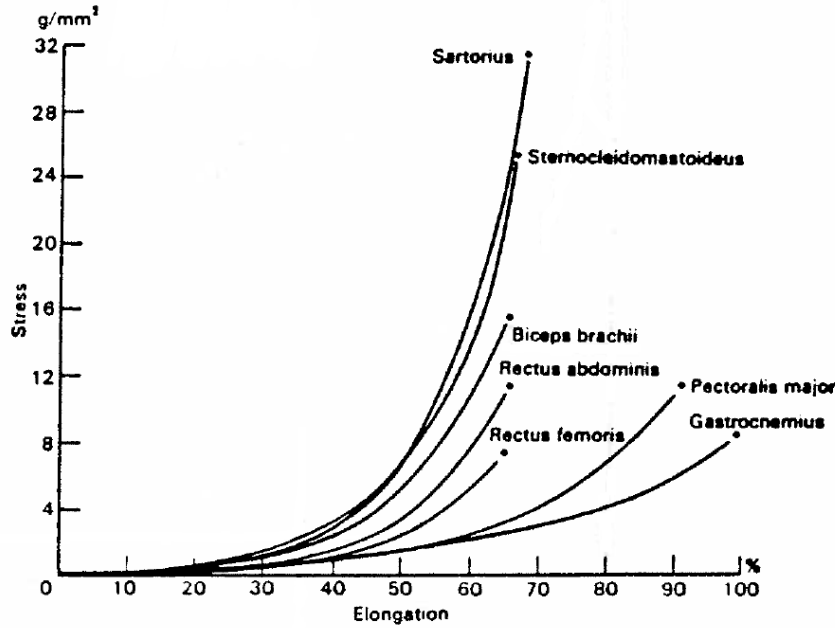
Figure 2.9: Stress-Strain curves in tension of passive skeletal muscle tissue of persons 29 years of age [18].

2.5.3 Constitutive model for viscous part

The constitutive model investigated in Section 2.5.2 was used to express the muscle constitutive model, excluding the viscous part. To add this part, the work by Limbert and Middleton [19] was studied, from which we used just the viscous contribution of the material model. Limbert and Middleton [19] presented in their work a transversely isotropic visco-hyper-elastic model with strain rate effect based on Helmholtz free energy and various invariants of $\boldsymbol{C}$-tensor. The total free energy function ψ was decomposed additively to equilibrium (elastic) and non-equilibrium (viscous) parts, ψ^e and ψ^v respectively, in a Lagrangian configuration

$$\psi[X,\boldsymbol{C},\dot{\boldsymbol{C}},\boldsymbol{K}] = \overbrace{\psi^e[X,\boldsymbol{C},\boldsymbol{K}]}^{\text{elastic part}} + \overbrace{\psi^v[X,\boldsymbol{C},\dot{\boldsymbol{C}},\boldsymbol{K}]}^{\text{viscous part}} \quad (2.40)$$

The elastic and viscous second Piola-Kirchhoff stress tensors can be defined as

$$\boldsymbol{S}^{e} = 2\frac{\partial \psi^{e}}{\partial \boldsymbol{C}}, \qquad \boldsymbol{S}^{v} = 2\frac{\partial \psi^{v}}{\partial \dot{\boldsymbol{C}}} \tag{2.41}$$

The free energy functions are defined based on 17 invariants, I_{1-5} and J_{1-12}. The suggested relation [19] for viscous contribution to the Helmholtz free energy function is

$$\psi^{v} = \psi(J_2, I_1, J_5, I_4) = \begin{cases} \eta_1 J_2(I_1 - 3) & if I_4 \leq 1 \\ \\ \eta_1 J_2(I_1 - 3) + \frac{1}{2}\eta_2 J_5(I_4 - 1)^2 & if I_4 > 1 \end{cases} \tag{2.42}$$

where η_1 and η_2 are material parameters, and invariants I_1, I_4, J_2 and J_5 are as follows

$$I_1 = tr\boldsymbol{C}, \quad I_4 = N_0 : \boldsymbol{C}, \quad J_2 = \frac{1}{2}(\mathbf{I} : \dot{\boldsymbol{C}}^2), \quad J_5 = \boldsymbol{K} : \dot{\boldsymbol{C}}^2 \tag{2.43}$$

This model is supposed to represent the viscous effect of both bulk material and collagen fibers, when stretched (uncrimped).

The second Piola-Kirchhoff viscous stress tensor associated with the above viscous energy function can be derived through taking derivatives with respect to invariants, giving the following relation:

$$\boldsymbol{S}^{v} = \begin{cases} 2[\eta_1(I_1 - 3)\dot{\boldsymbol{C}}] & if I_4 \leq 1 \\ \\ 2\left[\eta_1(I_1 - 3)\dot{\boldsymbol{C}} + \frac{1}{2}\eta_2(I_4 - 1)^2 \Upsilon_{n_0\dot{\boldsymbol{C}}}\right] & if I_4 > 1 \end{cases} \tag{2.44}$$

Where $\Upsilon_{n_0\dot{\boldsymbol{C}}}$ is defined as

$$\Upsilon_{n_0\dot{\boldsymbol{C}}} = n_0 \otimes \dot{\boldsymbol{C}} \cdot n_0 + n_0 \cdot \dot{\boldsymbol{C}} \otimes n_0 \tag{2.45}$$

2.6 Modeling of muscle fibers

To define the fiber direction in the muscle various methods have been suggested. Böl and Reese [20] have suggested a simplified model for defining fiber direction using mathematical relations. For a simple fusiform muscle with r_1 and r_2 as minimum and maximum radius, respectively, the muscle fibers are defined by the following curves

$$\Gamma(z, \alpha) = \begin{pmatrix} r(z)\cos\alpha \\ r(z)\sin\alpha \\ z \end{pmatrix} \tag{2.46}$$

The radial locatio of the fiber is determined by the angle α and $r(z)$ is the distance of the fiber from the z axis, located in the center of the muscle. The muscle length is defined between $z = -h$ and $z = h$. $r(z)$ is suggested to be defined by the following relation

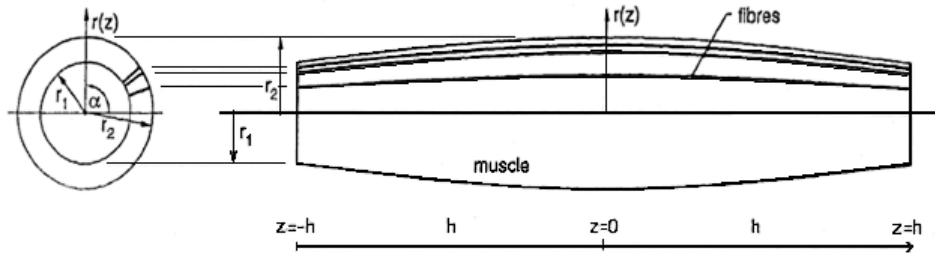$$r(z) = r_2 e^{-(z^2 ln(r_2/r_1)/h^2)} \tag{2.47}$$

Figure 2.10: the cross-section of a fusi-form muscle [20].

2.6.1 Definition of the fiber directions in the code

In the FE formulation for the MatLab code, three approaches for defining the fiber direction was implemented

• The first method that was tried was defining the directions based on the lines connecting the center of each element to the closer end point of the muscle. The simulations based on this fiber direction showed poor results in most cases. This is mainly due to the fact that the defined vectors for the elements closer to the end points of the muscle have directions mostly in transverse direction of the muscle, instead of being along the muscle, which is unrealistic. One way to improve the results is to define the vector directions pointing from the element center to a point a little outside of the muscle end, so that the the vectors become more directed along the muscle at ends.

• The second approach was an element-local definition, in which the fiber direction vectors were defined according to the lines connecting the center of the two opposite faces of each solid element. This provides vector direction for each element that somewhat follows the total shape of the muscle. Also more continuous vector field will be provided. This can be considered as the most general approach among the ones we have used, which can be implemented in muscles with different shapes.

• If the muscle structure is very simple and symmetric, a simple fiber direction vector can be defined based on the line going through both ends of the muscle. The simulations based on this method gave lower nodal forces. Although this is a rough estimation of the muscle fibers, in muscles with simple structures it can provide relatively satisfying results.

2.6.2 Fiber dispersion

If there is fiber dispersion in the muscle, a model should be presented in which the fiber direction can be expressed based on the fiber dispersion data. As mentioned before, Freed et al.[15] suggested a dispersion (anisotropic material stiffness) tensor, taking care of the muscle fiber direction. In global coordinate system, the matrix K has been defined as

$$\boldsymbol{K} = \boldsymbol{Q}\,\kappa\boldsymbol{Q}^{T} \tag{2.48}$$

where κ is the local (intrinsic) anisotropic matrix and $\boldsymbol{Q}$ is the an orthogonal transformation matrix. The matrix κ can be approximated as

$$\kappa = \frac{1}{2} \begin{bmatrix} 1 + e^{-2\sigma^2} & 0 & 0 \\ 0 & f(1 - e^{-2\sigma^2}) & 0 \\ 0 & 0 & (1 - f)(1 - e^{-2\sigma^2}) \end{bmatrix} \qquad (2.49)$$

Where σ is a phenomenological parameter similar to standard deviation which shows how the fiber directions are dispersed. For a 3D splay of muscle fibers $f = 1/2$ and for 2D case $f = 0$ and $f = 1$.

2.6.3 Localized activation

It should be noted that Equation 2.2 represents the force-velocity relation based on the total muscle velocity measured at the muscle end. In case of a continuum FE formulation, this relation can be expressed in terms of stretch rates at the Gauss points, derived from strain rate. Such a relation can be seen in Figure 2.11
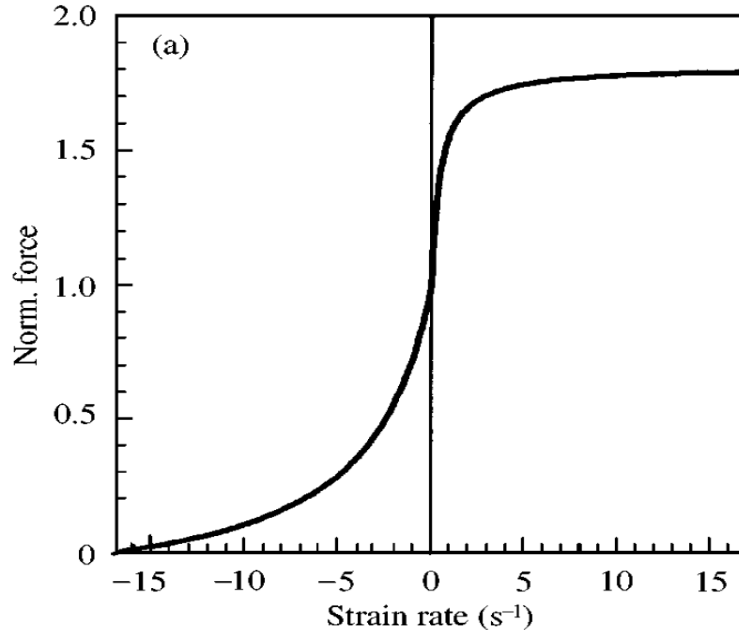
Figure 2.11: Force-Velocity relation (taken from Johansson et al. [21]).

In order to define the force-velocity relation, the local stretch rate of the muscle $\dot{\lambda}$ in each Gauss point should be determined. Having the fiber direction vector N_0 in the reference configuration, one can calculate $\dot{\lambda}$ using the following relations

$$\lambda^2 = \boldsymbol{N}_0^T \boldsymbol{C} \, \boldsymbol{N}_0 \qquad (2.50)$$

$$\frac{d(\lambda^2)}{dt} = 2\lambda\dot{\lambda} = \boldsymbol{N}_0^T \frac{d\boldsymbol{C}}{dt} \boldsymbol{N}_0 = \boldsymbol{N}_0^T \frac{d}{dt}(2\boldsymbol{E} + \boldsymbol{I}) \boldsymbol{N}_0 = 2\boldsymbol{N}_0^T \dot{\boldsymbol{E}} \, \boldsymbol{N}_0 = 2\boldsymbol{N}_0^T \boldsymbol{F}^T \boldsymbol{D} \, \boldsymbol{F} \, \boldsymbol{N}_0 \qquad (2.51)$$

$$\Rightarrow \dot{\lambda} = \frac{\boldsymbol{N}_0^T \boldsymbol{F}^T \boldsymbol{D} \, \boldsymbol{F} \, \boldsymbol{N}_0}{\lambda} \qquad (2.52)$$

3 FE formulation and implementation

For the numerical solution of our problem, a dynamic formulation has mainly been focused on. There are different methods for solution of such problems, depending on the condition of the problem, but two main approaches of numerical solutions can be mentioned, namely the explicit method and the implicit method.

3.1 A simple muscle model

In order to implement the FE formulations, a symmetric fusiform muscle was modeled in LS-PREPOST. This model was meshed using 96 eight node solid isoparametric elements, then the model geometry including the node numbering and coordinates were imported to the MatLab environment. Figure 3.1 illustrates the the model in both environments.
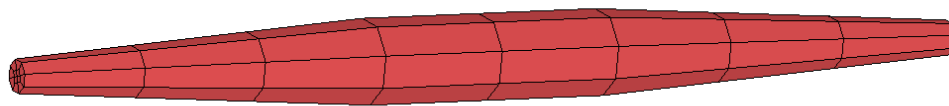
(a) Muscle model in LS-PREPOST.
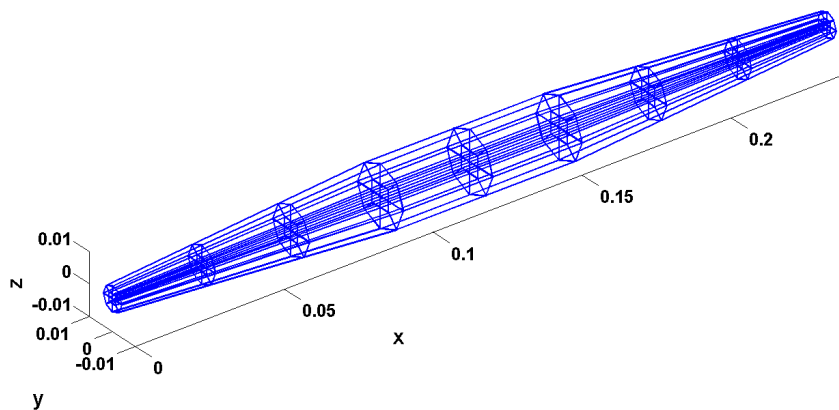
(b) Muscle model in MatLab.

Figure 3.1: The simple fusiform muscle plotted in (a) LS-PREPOST and (b) MATLAB.

As boundary conditions for the model, the left side of the model was constrained in all three translational directions using nodal constraint. The right side of the model was fixed in Y and Z direction, but free in X direction, letting the muscle end to move in the longitudinal direction.

3.2 Explicit method, central difference scheme

In case of short and fast events, explicit methods can be convenient; in fact, a short simulation time ensures that we do not have to run an excessive number of iterations while still having small time steps; consequently, we can accomplish our analysis within a reasonable number of iterations with an acceptable accuracy.

The semidiscrete momentum equation can be defined as

$$\boldsymbol{M}\,\ddot{d} + \boldsymbol{C}\,\dot{d} + f^{int}(d) = f^{ext} \tag{3.1}$$

where d is the displacement, $\ddot{d}$ and $\dot{d}$ are acceleration and velocity vectors respectively, $\boldsymbol{M}$ is the mass matrix and $\boldsymbol{C}$ is the damping matrix.

Central difference scheme: To comply with the LS-DYNA solution approach, this method, which is one of the most popular methods in computational mechanics among other methods, was chosen to be used in codes.

A difference formula is called explicit if the equation for the function at each time step involves only the derivatives at previous time steps [12]. Here, according to Belytschko et al.[12], the formulations for central difference method have been presented:

For a simulation time $0 \leq t \leq t_E$ subdivided into n time steps Δt^n, we can define the following relations:

$$\Delta t^{n+\frac{1}{2}} = t^{n+1} - t^n, \quad t^{n+\frac{1}{2}} = \frac{1}{2}(t^{n+1} + t^n), \quad \Delta t^n = t^{n+\frac{1}{2}} - t^{n-\frac{1}{2}} \tag{3.2}$$

With displacement vector d, velocity vector v and acceleration vector a, the central difference formula for the velocity is:

$$\dot{d}^{n+\frac{1}{2}} \equiv v^{n+\frac{1}{2}} = \frac{d^{n+1} - d^n}{t^{n+1} - t^n} = \frac{1}{\Delta t^{n+\frac{1}{2}}}(d^{n+1} - d^n) \tag{3.3}$$

This difference formula can be converted to an integration formula by rearranging the terms as follows:

$$d^{n+1} = d^n + \Delta t^{n+\frac{1}{2}} v^{n+\frac{1}{2}} \tag{3.4}$$

The velocities can be expressed at the midpoints of the time intervals, called half-steps. The acceleration and the corresponding integration formula are

$$\ddot{d}^n \equiv a^n = \left(\frac{v^{n+\frac{1}{2}} - v^{n-\frac{1}{2}}}{t^{n+\frac{1}{2}} - t^{n-\frac{1}{2}}} \right), \quad v^{n+\frac{1}{2}} = v^{n-\frac{1}{2}} + \Delta t^n a^n \tag{3.5}$$

By substituting (3.3) into (3.5), the acceleration can be expressed directly in terms of displacement:

$$\ddot{d}^n \equiv a^n = \frac{\Delta t^{n-\frac{1}{2}}(d^{n+1} - d^n) - \Delta t^{n+\frac{1}{2}}(d^n - d^{n-1})}{\Delta t^{n+\frac{1}{2}} \Delta t^n \Delta t^{n-\frac{1}{2}}} \tag{3.6}$$

In this work we have used equal time steps, so the above equation will be reduced to the following form

$$\ddot{d}^n \equiv a^n = \frac{(d^{n+1} - 2d^n + d^{n-1})}{(\Delta t^n)^2} \tag{3.7}$$

Next, for the nodal forces f^n and mass matrix $\boldsymbol{M}$, we can express the time integration of equation of motion at time step n

$$\boldsymbol{M}\, a^n = f^n = f^{ext}(d^n, t^n) - f^{int}(d^n, t^n) \tag{3.8}$$

Where f^{int} and f^{ext} are internal and external nodal forces, respectively

By substituting (3.8) into (3.5), the nodal velocities and displacements can be updated

$$v^{n+\frac{1}{2}} = v^{n-\frac{1}{2}} + \Delta t^n \boldsymbol{M}^{-1} f^n \tag{3.9}$$

Having the constitutive equation in terms of $\boldsymbol{D}^{\,n-\frac{1}{2}}$ and $\boldsymbol{E}^{\,n}$ and external nodal forces, f^n can be determined since the displacements d^n are known at each time step n. Consequently, $v^{n+\frac{1}{2}}$ can be evaluated, and using this, the displacement d^{n+1} can be found by (3.4). It should be noted that update of nodal velocities and displacements requires solution of no equation if the mass matrix $\boldsymbol{M}$ is diagonal [12].

3.2.1 Implementation and flowchart

The finite element formulation for implementation in Matlab codes have been developed based on the flowchart for explicit time integration presented by Belytschko et al. [12]. This flowchart provides a solution for a dynamic problem with a damping matrix modeled by linear viscous force $f^{damp} = C^{damp}v$. The velocity is updated in two steps:

$$v^n = v^{n-\frac{1}{2}} + (t^n - t^{n-\frac{1}{2}})a^n, \quad v^{n+\frac{1}{2}} = v^n + (t^{n+\frac{1}{2}} - t^n)a^n \tag{3.10}$$

The flowchart for explicit time integration is as follows

1. Initial conditions and initialization:
   set v^0, σ^0, and initial values of other material state variables;
   $d^0 = 0$, $n = 0$, $t = 0$; compute $\boldsymbol{M}$

2. *getforce*

3. Compute accelerations $a^n = \boldsymbol{M}^{-1}(f^n - \boldsymbol{C}^{\,damp}v^{n-\frac{1}{2}})$

4. Time update: $t^{n+1} = t^n \Delta t^{n+\frac{1}{2}}, t^{n+\frac{1}{2}} = \frac{1}{2}(t^n + t^{n+1})$

5. First partial update nodal velocities: $v^{n+\frac{1}{2}} = v^n + (t^{n+\frac{1}{2}} - t^n)a^n$

6. Enforce velocity boundary conditions

7. Update nodal displacements: $d^{n+1} = d^n + \Delta t^{n+\frac{1}{2}}v^{n+\frac{1}{2}}$

8. *getforce*

9. Compute a^{n+1}

10. Second partial update of nodal velocities: $v^{n+1} = v^{n+\frac{1}{2}} + (t^{n+1} - tn + \frac{1}{2})a^{n+1}$

11. Update counter: $n + 1 \to n$

12. Output; if simulation not complete, go to 4.

Subroutine *getforce*

1. Initialization: $f^n = 0, \quad \Delta t_{crit} = \infty$

2. Compute global external nodal forces f^n_{ext}

3. Loop over element e

    i Gather element nodal displacement and velocities

    ii $f^{int,n}_e = 0$

    iii Loop over quadrature points ξ_Q

        1 if $n = 0$, go to 4

        2 compute measures of deformation: $\boldsymbol{D}^{\,n-\frac{1}{2}}(\xi_Q), \boldsymbol{F}^{\,n}(\xi_Q), \boldsymbol{E}^{\,n}(\xi_Q)$

        3 compute stress $\sigma^n(\xi_Q)$ by constitutive equation

        4 $f^{int,n}_e \leftarrow f^{int,n}_e + B^T \sigma^n \bar{w}_Q J \mid_{\xi_Q}$
        END quadrature point loop

    iv Compute external nodal forces on element, $f^{ext,n}_e$

    v $f^n_e = f^{ext,n}_e - f^{int,n}_e$

    vi Compute $\Delta t^e_{crit}, \quad$ if $\quad \Delta t^e_{crit} < \Delta t_{crit} \quad then \quad \Delta t_{crit} = \Delta t^e_{crit}$

    vii scatter f^n_e to global f^n

4. END loop over elements

5. $\Delta t = \alpha \Delta t_{crit}$

3.3 Implicit method

The implicit method is more complicated, mainly due to calculation of the tangent modulus, but if convergence is achieved, it gives more reliable results compared to the explicit method. This method involves solution of non-linear algebraic equations. Among solution methods, the most popular and robust method is Newton's method.

In Belytschko et al.[12] a brief description of this method is provided, which is summarized in the following:

A general one dimensional non-linear algebraic equation based on the equation of motion, expressed in form of Newmark β-equation is

$$0 = r = \frac{1}{\beta \Delta t^2} \boldsymbol{M} \left(d^{n+1} - \tilde{d}^{n+1} \right) - f^{ext}(d^{n+1}, t^{n+1}) + f^{int}(d^{n+1}) \tag{3.11}$$

Where r is the residual, β is a Newmark parameter, and $\tilde{d}^{n+1}$ and d^{n+1} are defined as follows

$$d^{n+1} = \tilde{d}^{n+1} + \beta \Delta t^2 a^{n+1} \qquad where \qquad \tilde{d}^{n+1} = d^n + \Delta t v^n + \frac{\Delta t^2}{2}(1 - 2\beta)a^n \tag{3.12}$$

$$v^{n+1} = \tilde{v}^{n+1} + \gamma \Delta t a^{n+1} \qquad where \qquad \tilde{v}^{n+1} = v^n + (1 - \gamma)\Delta t a^n \tag{3.13}$$

where γ is also a Newmark parameter.

The iteration number is i: $d_i^{n+1} \equiv d_i$ is the displacement in iteration i at time step $n+1$

A Taylor expansion of the residual about the current nodal displacement with dropped higher order derivatives gives the following linearized model:

$$0 = r(d_i, t^{n+1}) + \frac{\partial r(d_i, t^{n+1})}{\partial d} \Delta d \tag{3.14}$$

Solving the above equation for incremental displacement gives

$$\Delta d = - \left(\frac{\partial r(d_i)}{\partial d} \right)^{-1} r(d_i) \tag{3.15}$$

To solve a non-linear equation, a sequence of linear models should be solved in an iterative manner until a convergence is achieved. In each iteration the unknown d value is updated using

$$d_{i+1} = d_i + \Delta d \tag{3.16}$$

In matrix form, the matrix $\partial r / \partial d$ is called the system Jacobian matrix or effective tangent stiffness and denoted by A:

$$A = \frac{\partial r}{\partial d} \tag{3.17}$$

So we will have

$$r + A \Delta d = 0 \tag{3.18}$$

Flowchart: The flowchart shows a full Newton algorithm, where the Jacobian matrix is evaluated and inverted in each iteration. The implicit algorithm begins with applying initial conditions. To begin each iterative procedure, a starting value of d is needed which usually the solution from the previous time step is used. The Jacobian is calculated for the latest state of the body.

1. Initial conditions and initialization of parameters:
   set v^0 , σ^0 ; $d^0 = 0, t = 0$; compute $\boldsymbol{M}$

2. Get $f^0 = f(d^0, 0)$

3. Compute initial accelerations $a^n = \boldsymbol{M}^{-1} f^n$

4. Estimate next solution: $d_{new} = d^n$ or $d_{new} = \tilde{d}^{n+1}$

5. Newton iterations for time step $n + 1$:

   (a) *getforce* computes $f(d_{new}, t^{n+1})$
   (b) $a^{n+1} = 1 / \beta \Delta t^2 (d_{new} - \tilde{d}^{n+1}), v^{n+1} = \tilde{v}^{n+1} + \gamma \Delta t a^{n+1}$
   (c) $r = \boldsymbol{M} a^{n+1} - f$
   (d) Compute Jacobian A(d)
   (e) Modify A(d) for essential boundary conditions

(f) solve linear equations $\Delta d = -A^{-1}r$

(g) $d_{old} + \Delta d \rightarrow d_{new}$

(h) Check convergence criterion; if not met, go to step 5a.

6. Update displacements, counter and time: $d^{n+1} = d_{new}, n + 1 \rightarrow n, t + \Delta t \rightarrow t$

7. Check energy balance

8. Output; if simulation not complete, go to 4

3.4 Numerical problems

3.4.1 Incompressibility/nearly-incompressibility

The muscle tissue is composed of about 70% water [15] which means that the muscle tissue can be considered as a nearly-incompressible material. In fact, the bulk modulus of the material is significantly larger than shear modulus. For an incompressible material the poisson ratio is 0.5, and materials with poisson ratios greater than 0.4 can be considered to be nearly-incompressible [22]. In these cases, instabilities or volume locking in the elements can happen.

3.5 Problem treatments

3.5.1 Reduced-selective method

For a nearly incompressible material like muscle tissue, element locking can happen, which means that the displacements of some elements are very small, so that very slow or even no convergence can be obtained.

One solution for this numerical problem is that the volumetric and deviatoric parts of the stress matrix are separated, and when performing the numerical quadrature, the pressure (volumetric stress) is under-integrated, while the deviatoric part is fully integrated.

$$\sigma_{ij} = \sigma_{ij}^{dev} + \sigma^{hyd}\delta_i j \tag{3.19}$$

Where

$$\sigma^{hyd} = \frac{1}{3}\sigma_{kk} = -p, \qquad \sigma_{ij}^{dev} = \sigma_{ij} - \sigma^{hyd}\delta_i j \tag{3.20}$$

The expression for selective-reduced integration of the internal forces is [12]

$$(f_{iI}^{int})^T = f_{Ii}^{int} = -J_\xi(0)N_{I,i}(0)p(0) + \sum_{Q=1}^{4} \bar{w}_Q J_\xi(\xi_Q)N_{I,j}(\xi_Q)\sigma_{ji}^{dev}(\xi_Q) \tag{3.21}$$

In the above equations, I is the node number and N is shape function. For more details see Belytschko et al. [12].

3.5.2 Two-Field/ Three-Field Formulation

The main problem with incompressible or nearly incompressible problems stems from determination of pressure field corresponding to volumetric strain. To circumvent this problem, it is convenient to separate the pressure and consider it as an independent variable [22].

In case of nearly-incompressible problems, sometimes it is appropriate to apply a three-field approach, where beside pressure field as an independent degree of freedom, an extra field corresponding to the minor volumetric strain is added. It should be noted that volume-changing deformations require much higher external work than deviatoric deformations, so ignoring this part will produce a significant amount of error in the results.

3.5.3 Rayleigh damping

Another mechanism to cope with the unstable simulation results is using a damping matrix in the equation of motion (see the flowchart for the explicit time integration). The Rayleigh damping can be computed as

$$\boldsymbol{C} = \alpha \boldsymbol{M} + \beta \boldsymbol{K} \tag{3.22}$$

where $\boldsymbol{M}$ and $\boldsymbol{K}$ are mass and stiffness matrices, respectively, and α and β are coefficients. By manipulating these coefficients, the desired amount of damping in the solution can be achieved. LS-DYNA also uses a similar damping effect in its simulations to control numerical instabilities.

4 Numerical simulations and results

In this section, the simulation of the isometric tests of the muscle with different conditions is focused on. The right end of the muscle was rapidly displaced to a pre-determined length, and after the dynamic response had settled, the isometric force was recorded. By conducting this test for a range of stretches, the curves of the cross-sectional force with respect to the muscle stretch were plotted. The simulation was performed for passive, as well as the total force of the muscle. In the ideal case, the resulting curve is expected to resemble the curve in Figure 2.4.

4.1 Simulation for passive force

The model was stretched in small intervals without the activation. After achieving stationary state in each stretch interval, the cross-sectional force in the muscle model was recorded. As can be seen from the Figure 4.1, the results show good agreement with expected exponential function defined for the passive force.
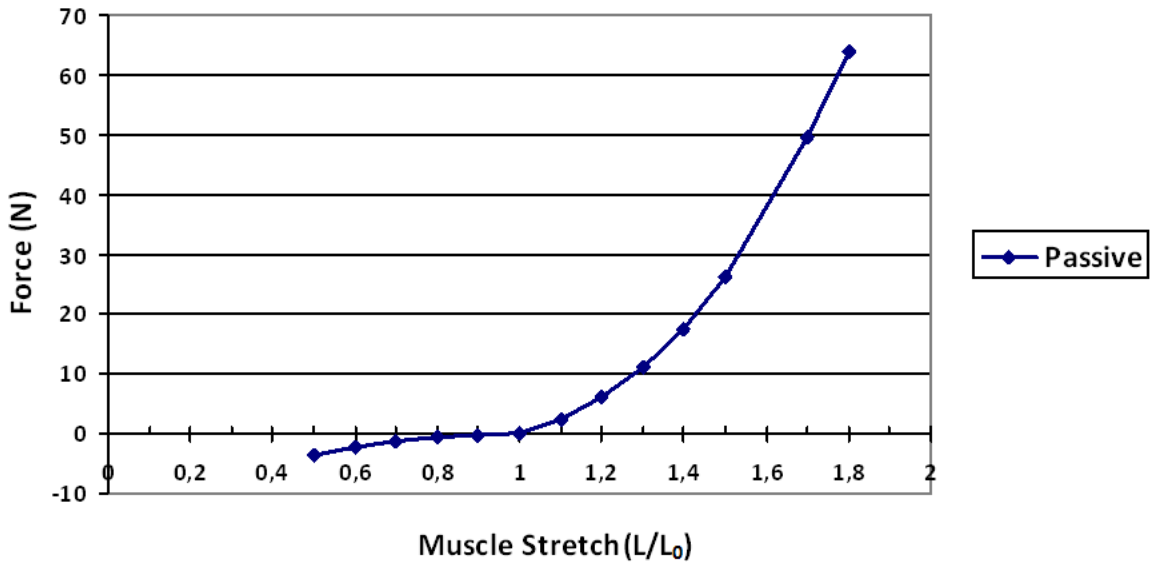
Figure 4.1: Muscle passive force with respect to the stretch in the fiber direction.

4.2 Simulation with element-local definitions

In this simulation, an element-local definition of the fiber direction (cf. Section 2.6.1), connecting centers of opposing faces of each element, was used. Also, the local stretch rate was employed as a measurement for evaluation of the F_V function. The results are shown in Figure 4.2.
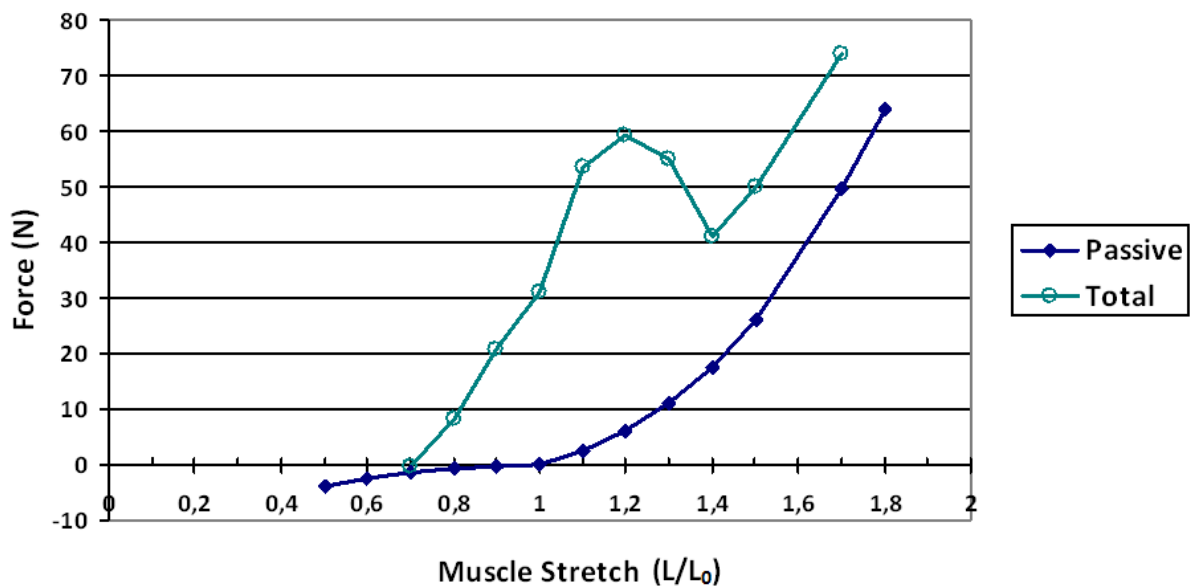

Figure 4.2: Active force for the model with fibers defined by the line connecting the center of the opposing faces of each element.

The resulting graph shows some over-estimation of the active force, specially in the

stretched part of the graph. It was expected that the curve of total force be fitted on the passive curve in the stretch region of more than 1.5 since there is almost no active force generated with stretches more than this amount, but we got higher values.

This result can be explained with respect to the model geometry we have used. Being fusiform, the model has different cross-sectional areas, leading to different amounts of stiffness. In fact, when a specific amount of the stretch has been applied, the elements near to the two ends of the muscle will be stretched much more than the elements in the middle due to their lower stiffness; consequently, the elements in excessive stretch state will generate little or no active force while their passive response is high. On the other hand, the elements more to the center can still have very small stretch making them able to produce almost the maximum of their active force. As a result, the cross-sectional force of the whole muscle will be higher than the expected values. In reality, it seems that muscles have varying stiffness with respect to their cross-sectional area such that they are stiffer at ends to compensate for the reduced area.

4.3   Simulation with modified geometry

Due to the problems with the fusiform geometry, a modified model was used for simulation. This model has a cylinder-like geometry with a smaller reduction in area at ends (Figure 4.3). Using this model, less variation in the stiffness of the model along the muscle model is expected.

The other modification was replacement of F_L curve with a wider curve (4.1)(Figure 4.4) taken from Böl and Reese [20]. Using this curve, elements will experience less intense changes around the L_0 leading to more stable condition.

$$f_\lambda(\lambda_{fiber}) = \begin{cases} 0 & \lambda_{fiber} < 0.4\lambda_{opt} \\[2mm] 9(\frac{\lambda_{fiber}}{\lambda_{opt}} - 0.4)^2 & 0.6\lambda_{opt} > \lambda_{fiber} \geq 0.4\lambda_{opt} \\[2mm] 1 - 4(1 - \frac{\lambda_{fiber}}{\lambda_{opt}})^2 & 1.4\lambda_{opt} > \lambda_{fiber} \geq 0.6\lambda_{opt} \quad , \qquad \lambda_{opt} = 1 \\[2mm] 9(\frac{\lambda_{fiber}}{\lambda_{opt}} - 1.6)^2 & 1.6\lambda_{opt} > \lambda_{fiber} \geq 1.4\lambda_{opt} \\[2mm] 0 & \lambda_{fiber} \geq 1.6\lambda_{opt} \end{cases} \qquad (4.1)$$

The simulation results showing the passive and total forces is illustrated in Figure 4.5
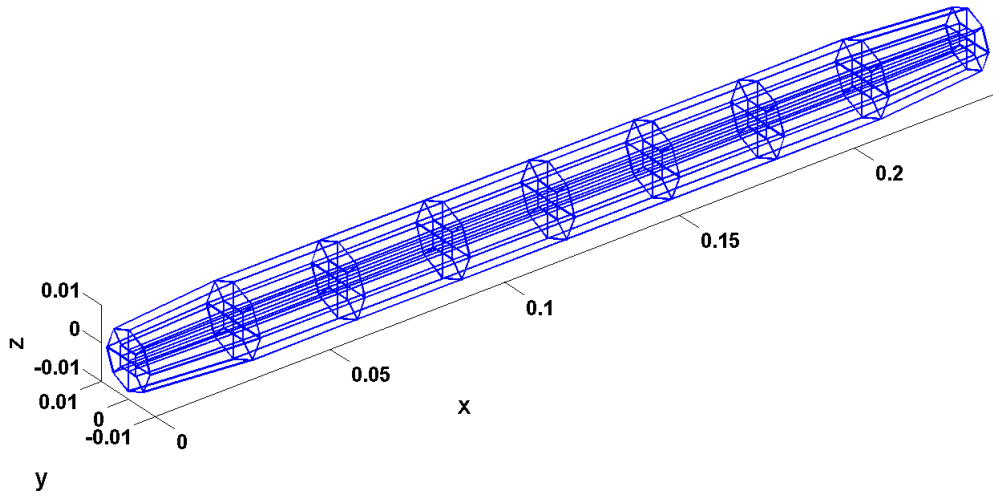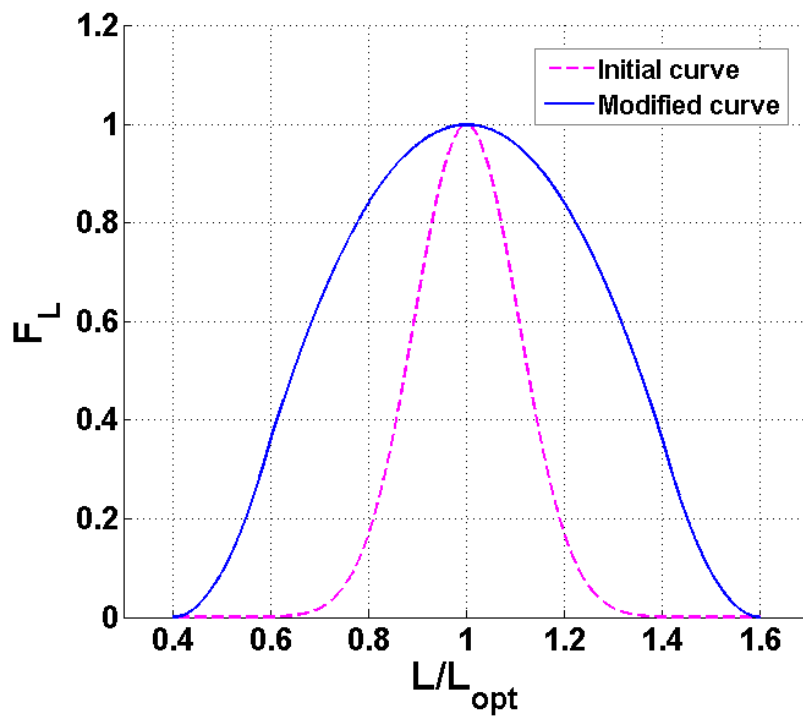
Figure 4.3: The modified geometry.

Figure 4.4: Comparison between two F_L curves; the wider curve is taken from [20].
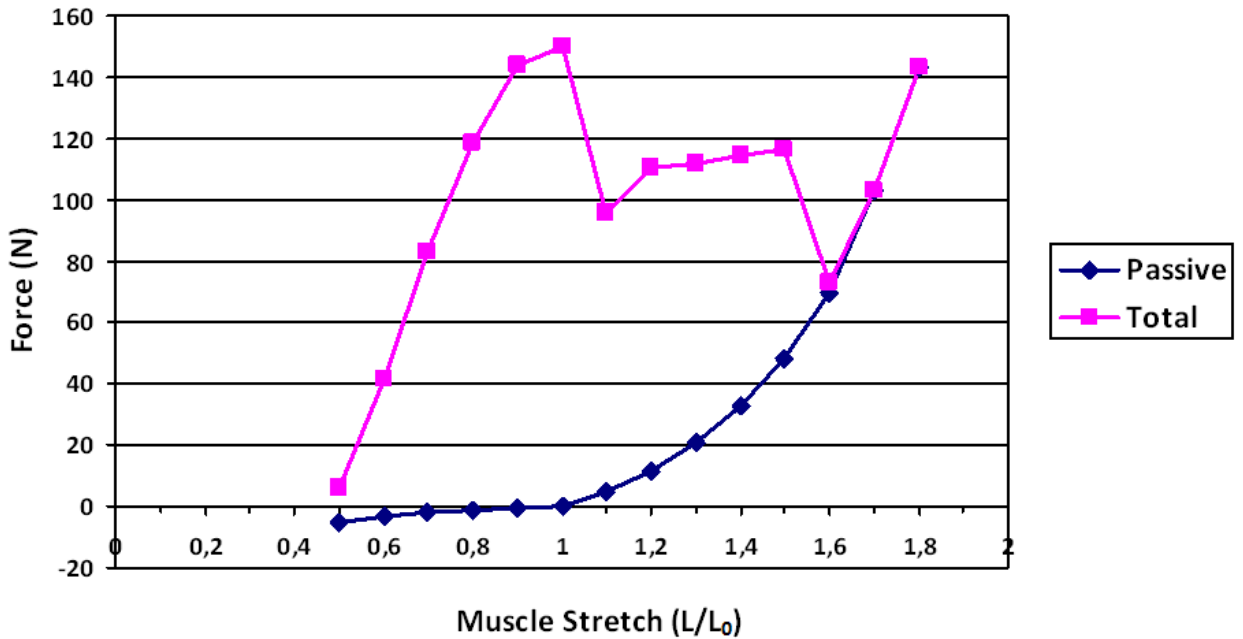
Figure 4.5: The results for the modified geometry.

The curves in Figure 4.5 shows improved results. The curve for the total force now fits the passive curve, but for stretch values between 1.1 and 1.5 we still got higher values than expected.

4.4 Simulation with global Hill's formulation

Many attempts to simulate the muscle behavior based on pure continuum modeling with local definition of the variables led to some numerical errors, as was shown in the examples in Section 4.2 and 4.3. In order to have more clear comparison, this time the velocity and displacement of the whole muscle at its right end was measured to be used for evaluation of the F_V and F_L functions for the all integration points.
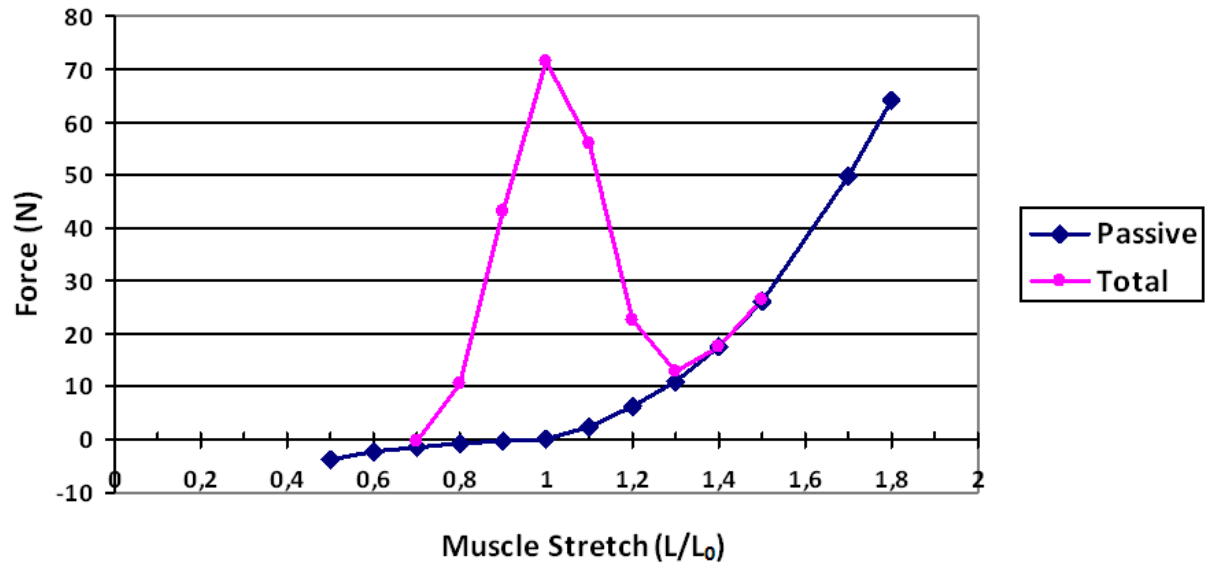
Figure 4.6: The results for simulation with considering the whole muscle as one Hill's element.

As can be seen from Figure 4.6 much better results was achieved. Overall trend of the curve has a good agreement with the expected curve.

4.5 Table of papers

In this section, based on the studied literature, a brief summary have been provided in tabular form where the relevant and useful aspects of each study material have been pointed out.

Table 4.1: Reviewed continuum muscle models in the literature.

Author and Year	Numerical method	Material model	Activation model	Incompressibility
Almeida and Spilker, 1997 [23]	Implicit finite difference Newton-Raphson	Transversely isotropic hyperelastic	N/A	Two field, fully incompressible
Böl and Reese, 2007 [20]	N/A	Neo-Hookean	Hill's model	Nearly incompressible
Freed et al., 2005 [15]	Forward Euler integration	Transversely isotropic Mooney material	N/A	Nearly incompressible
Hedenstierna et al., 2008 [5]	N/A	Visco-hyperelastic	Hill's model	Nearly incompressible
Ito et al., 2009 [24]	N/A	Transversely isotropic viscoelastic	Active part of the free energy	Single field, Nearly incompressible
J. M. Guccione et al., 1993, Part 1,2 [8]	Range Kutta	Anisotropic hyperelastic	Calcium ion concentration	Incompressible
Johansson et al., 2000 [21]	Newton iterative method	Hyperelastic	Hill's model	Nearly incompressible
Kaliske and Rothert, 1997 [25]	Newton iterative method	isotropic viscoelastic	N/A	N/A
Kaliske, 1999 [14]	Newton iterative method	Transversely isotropic viscoelastic	N/A	Nearly incompressible
Limbert and Middleton, 2004 [19]	Explicit Fast Deformation	Transversely isotropic Visco-hyperelastic	N/A	Two-field, fully incompressible
Martins et al.,1998 [9]	Explicit	Transversely isotropic hyperelastic	Series element in Hill's model	Quasi incompressible
Martins et al., 2006 [26]	Explicit	Transversely isotropic hyperelastic	Hill's model	Two field, fully incompressible
Ning et al., 2006 [27]	Explicit integration scheme	Transversely isotropic viscoelastic	N/A	Nearly incompressible

Author, Year	Numerical Method	Material Model	Activation Model	Incompressibility
Olsson, 2009 [16]	Explicit	Transversely isotropic Neo-Hookian material	Calcium concentration	Nearly incompressible
Oomens et al.,2003 [10]	Implicit, quasi-static	Anisotropic Neo-Hookian	Huxley model,two state	Two field, fully incompressible
Pena et al., 2007 [28]	Newton iterative method	Anisotripic viscohyperelastic Kelvin-Voigt	N/A	Two field, fully incompressible
Pena et al., 2010 [29]	Newton iterative method	Anisotropic visco-hyperelastic	N/A	Quasi-incompressible
Pioletti et al., 1998 [30]	Explicit	Viscoelastic	N/A	Two field, fully incompressible
Reese and Govindjee, 1998 [31]	Newton iterative method	Finite Deformation Viscoelasticity	N/A	N/A
Stålhand et al., 2007	Mechanochemical	N/A	Calcium ion concentration	N/A
Yucesoy et al., 2002 [32]	Two-domain approach	anisotropic	Length dependency	Incompressible solid

5 Discussion

Considering the achieved results in the previous section, by evaluating the F_V and F_L using velocity and displacement measured at the muscle end, global Hill's formulation, much better results were obtained, and since the Hill's equation is defined based on the whole muscle length and velocity, it is more compatible with this simulation approach. On the other hand, using a "total continuum" approach, with all variables defined locally, seems to have some limitations. Over-estimation of the forces and more unstable results can be mentioned as examples of such problems.

Applying Hill-based relations to each of the elements can also lead to numerical errors which are more dependent on testing condition. For instance, these kinds of simulations are sensitive to the manner of application of the initial conditions. In this case consider the isometric tests of the muscle in which stretch intervals are applied to the muscle end (cf. Section 4). This stretch intervals should be applied gradually within 150 ms, for example. In case of fast stretch application, the elements adjacent to the right-hand-side of the muscle will be stretched too much while the other elements do not have enough time to respond to this stretch; in other words, the applied displacement do not propagate fast enough. This makes the elements with excessive stretches generate little active force and the other elements with little stretches generate almost the maximum of their active force. Consequently, the activated muscle will get an asymmetric shape with inaccurate amount of forces.

One of the numerical problems that may arise is related to non-unique equilibrium points. This problem is demonstrated in figure 5.1.
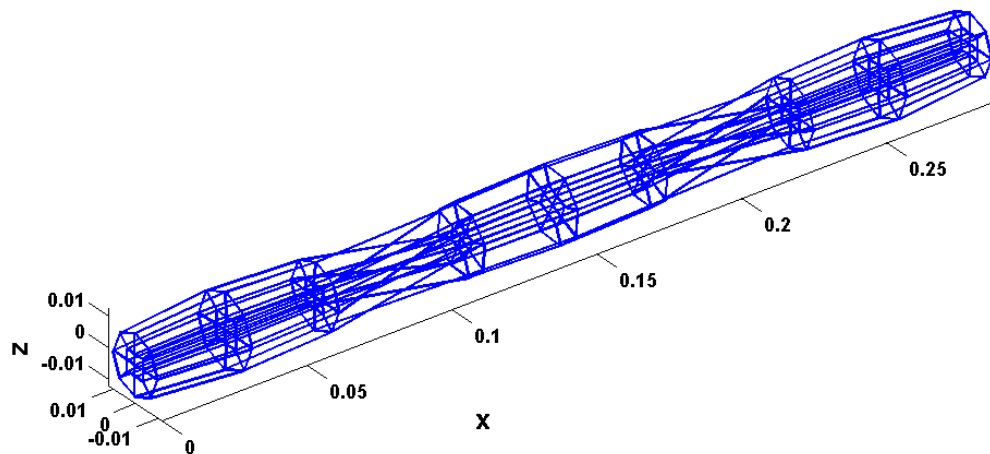

Figure 5.1: A simple cylindrical model stretched and activated.

This figure shows a simple cylindrical model, stretched by 1.2 and activated. Comparing the cross-sectional area of the tips with neighboring cross-sections one can notice that the inner cross-sections have larger areas that implies compressed state of the corresponding elements. This phenomenon can be explained by considering Figure 2.4. As can be seen from this figure, for a specific amount of force the muscle can have two amounts of stretch, one in compressed state and one in stretched state. It is possible for some elements to

find their equilibrium point in a compressed state despite the fact that the whole muscle is stretched.

Concerning the geometry dependency of the simulations, having more elaborate model with varying stiffness seems necessary. To mimic the configuration of a real muscle the model can be composed of different sections with different material properties. In the simulations performed in this work, a rigid body was assumed to be interacting with both ends of the muscle, but to have more realistic model, it is convenient that the tendon tissue is also taken into account. An elastic material can represent the tendon tissue.

6 Future Work

Based on the research done so far, and the problems that we encountered during the analyses, a number of future work have been suggested here to dig into the problem and improve the results.

Implicit Method: Since the explicit method is more likely to give unstable results, implicit method can be used as an alternative. Specifically, there are many papers in which implicit method has been implemented. Although this method is more computationally demanding, the achieved results will be more reliable, on condition that the convergence is obtained in each time step.

Other Explicit Methods: For the materials with fast varying stiffness, Runge-Kutta method may be suitable to be used instead of central difference scheme since in some cases the accuracy of central difference method can be inadequate [12].

Micro-scale investigation of muscles: In order to establish a continuum model of the muscle tissue, a local definition of muscle activation mechanism is needed. It is more convenient to have access to experimental data of the muscle in micro-scale level, or activation models defined in local fashion.

Generalization of fiber definition: Since the developed material model is supposed to be implemented for skeletal muscles of different shapes, more effort can be devoted to the definition of a fiber direction that is mesh independent, and can be implemented in various shapes of muscles.

Porous media theory: The muscle tissue has characteristics that could be modeled more efficiently using the porous media theory. When stress is developed in the muscle, some fluid migration can occur inside the tissue which can be responsible for the viscosity of the muscle in different directions, so one can try to model this behavior by a porous material with two phases of solid and fluid.

Handling numerical problems: Due to nearly incompressibility of the muscle material, numerical problems such as instabilities and volume locking are usually possible to occur in the simulations. One of the most common approaches for coping with such problems is using two-field or three-field methods that can be focused on in the future.

Experimental Data: In this project there was a need to have a comprehensive set of experimental data to calibrate the formulations and verify the results. If these data are provided, more detailed simulations with different test conditions can performed, and more comparison with experimental data can be done.

References

[1] J. O. Hallquist. *LS-DYNA Theory Manual*. Livermore Software Technology Corporation, Livermore, California, USA, 2006.

[2] Y. C. Fung. *Biomechanics - Mechanical Properties of Living Tissues*. Springer-Verlag, New York, USA, 2nd edition, 1993.

[3] J.M. Winters and L. Stark. Estimated mechanical properties of synergistic muscles involved in movements of a variety of human joints. *Journal of Biomechanics*, 21(12):1027–1041, 1988.

[4] F.E. Zajac. Muscle and tendon: properties, models, scaling, and application to biomechanics and motor control. *Critical reviews in biomedical engineering*, 17(4):359, 1989.

[5] S. Hedenstierna, P. Halldin, and K. Brolin. Evaluation of a combination of continuum and truss finite elements in a model of passive and active muscle tissue. *Computer Methods in Biomechanics and Biomedical Engineering*, 11(6):627–639, 2008.

[6] S.I. Murtada, M. Kroon, and G.A. Holzapfel. A calcium-driven mechanochemical model for prediction of force generation in smooth muscle. *Biomechanics and Modeling in Mechanobiology*, pages 1–14.

[7] J. Stålhand, A. Klarbring, and G.A. Holzapfel. Smooth muscle contraction: Mechanochemical formulation for homogeneous finite strains. *Progress in biophysics and molecular biology*, 96(1-3):465–481, 2008.

[8] J.M. Guccione, L.K. Waldman, and A.D. McCulloch. Mechanics of active contraction in cardiac muscle: Part 2 Cylindrical models of the systolic left ventricle. *Journal of biomechanical engineering*, 115:82, 1993.

[9] J.A.C. Martins, EB Pires, R. Salvado, and PB Dinis. A numerical model of passive and active behavior of skeletal muscles. *Computer methods in applied mechanics and engineering*, 151(3-4):419–433, 1998.

[10] C. W. J. Oomens, M. Maenhout, C. H. Van Oijen, M. R. Drost, and F. P. Baaijens. Finite element modelling of contracting skeletal muscle. *Philosophical Transactions of the Royal Society of London. Series B: Biological Sciences*, 358(1437):1453, 2003.

[11] A.J. Van den Bogert, K.G.M. Gerritsen, and G.K. Cole. Human muscle modelling from a user's perspective. *Journal of Electromyography and Kinesiology*, 8(2):119–124, 1998.

[12] T. Belytschko, W. K. Liu, and B. Moran. *Nonlinear Finite Elements for Continua and Structures*. John Wiley & Sons, Ltd, England, 2000.

[13] J. Bonet and R. D. Wood. *Nonlinear Continuum Mechanics for Finite Element Analysis*. Cambridge University Press, New York, USA, 2nd edition, 2008.

[14] M. Kaliske. A formulation of elasticity and viscoelasticity for fibre reinforced material at small and finite strains. *Computer methods in applied mechanics and engineering*, (185), 1999.

[15] A.D. Freed, D.R. Einstein, and I. Vesely. Invariant formulation for dispersed transverse isotropy in aortic heart valves. *Biomechanics and modeling in mechanobiology*, 4(2):100–117, 2005.

[16] T. Olsson. A new material model in ls-dyna: an anisotropic dispersed fiber model with actvation, 2009.

[17] U. Brink and E. Stein. On some mixed finite element methods for incompressible and nearly incompressible finite elasticity. *Computational Mechanics*, 19(1):105–119, 1996.

[18] H. Yamada and F.G. Evans. *Strength of biological materials*. Williams & Wilkins, 1970.

[19] G. Limbert and J. Middleton. A transversely isotropic viscohyperelastic material:: Application to the modeling of biological soft connective tissues. *International journal of solids and structures*, 41(15):4237–4260, 2004.

[20] M. Böl and S. Reese. Micromechanical modelling of skeletal muscles based on the finite element method. *Computer methods in biomechanics and biomedical engineering*, 11(5):489–504, 2008.

[21] T. Johansson, P. Meier, and R. Blickhan. A finite-element model for the mechanical analysis of skeletal muscles. *Journal of theoretical biology*, 206(1):131–149, 2000.

[22] O.C. Zienkiewicz and R.L. Taylor. *The finite element method. The Basis. Volume 1*. Butterworth-Heinemann, 2000.

[23] E.S. Almeida and R.L. Spilker. Mixed and penalty finite element models for the nonlinear behavior of biphasic soft tissues in finite deformation: part I-alternate formulations. *Computer methods in biomechanics and biomedical engineering*, 1(1):25–46, 1997.

[24] D. Ito, E. Tanaka, and S. Yamamoto. A novel constitutive model of skeletal muscle taking into account anisotropic damage. *Journal of the Mechanical Behavior of Biomedical Materials*, 3(1):85–93, 2010.

[25] M. Kaliske and H. Rothert. Formulation and implementation of three-dimensional viscoelasticity at small and finite strains. *Computational Mechanics*, 19(3):228–239, 1997.

[26] J.A.C. Martins, M.P.M. Pato, and E.B. Pires. A finite element model of skeletal muscles. *Virtual and Physical Prototyping*, 1(3):159–170, 2006.

[27] X. Ning, Q. Zhu, Y. Lanir, and S.S. Margulies. A transversely isotropic viscoelastic constitutive equation for brainstem undergoing finite deformation. *Journal of biomechanical engineering*, 128:925, 2006.

[28] E. Peña, B. Calvo, MA Martínez, and M. Doblaré. An anisotropic visco-hyperelastic model for ligaments at finite strains. Formulation and computational aspects. *International Journal of Solids and Structures*, 44(3-4):760–778, 2007.

[29] E. Peña, B. Calvo, M.A. Martínez, P. Martins, T. Mascarenhas, R.M.N. Jorge, A. Ferreira, and M. Doblaré. Experimental study and constitutive modeling of the viscoelastic mechanical properties of the human prolapsed vaginal tissue. *Biomechanics and Modeling in Mechanobiology*, 9(1):35–44, 2010.

[30] D.P. Pioletti, L.R. Rakotomanana, J.F. Benvenuti, and P.F. Leyvraz. Viscoelastic constitutive law in large deformations application to human knee ligaments and tendons. *Journal of Biomechanics*, 31(8):753–757, 1998.

[31] S. Reese and S. Govindjee. A theory of finite viscoelasticity and numerical aspects. *International Journal of Solids and Structures*, 35(26):3455–3482, 1998.

[32] C.A. Yucesoy, B.H. Koopman, P.A. Huijing, and H.J. Grootenboer. Three-dimensional finite element modeling of skeletal muscle using a two-domain approach: linked fiber-matrix mesh model. *Journal of biomechanics*, 35(9):1253–1262, 2002.